

SUPPLEMENTAL MATERIAL

Expanded Methods

Echocardiography

Measurements of dimensional and functional parameters were performed at baseline, before mice entered the treatment, and every 4 weeks thereafter, using a high-frequency, high resolution echocardiography system (Vevo 660, Visual Sonics, Toronto, Canada). Briefly, mice were anesthetized using tribromo-ethanol and transferred to an imaging stage equipped with a warming pad for controlled maintenance of mouse body temperature at 37° C and a built-in electrocardiography system for continuous heart rate (HR) monitoring. Standard B mode (2D) images of the heart and pulsed Doppler images of the mitral valve inflow were acquired. The thickness of the left ventricle (LV) was measured at the level of the papillary muscles in parasternal short axis at end-systole and end-diastole. LV ejection fraction (LVEF) and fractional shortening (LVFS) were determined as described by De Simone *et al.*¹

Measurement of intra-ventricular pressure

Terminal measurement of left ventricular pressure (LVP) was made at 20 weeks after DM induction in type-1 diabetic mice (n=12 in each group) and at 17 weeks of age in type-2 diabetic mice (n=10 in each group). The body temperature of the mice was maintained between 36° and 37° C throughout the experiment using a homeothermic blanket warming system. A tracheotomy was made and the mouse was intubated using the 23 gauge catheter, secured in place with 6-0 silk suture.

A high-fidelity 1.4F transducer tipped catheter (Millar Instruments, Houston, TX, USA) was zeroed in 37°C saline. Calibration of the transducer was verified using a mercury manometer, as suggested by the manufacturer. The right carotid artery was isolated, and tow ties were gently pulled back, using hemostats, to block blood flow from vessel. When pulsatile flow was no longer visible, a small cut was made just below the distal tie, and the catheter was placed inside the carotid artery and secured in place. The transducer was advanced into the heart, where its

position was confirmed by the rapid deflection of the diastolic pressure wave without any change in systolic pressure. Mice were allowed to stabilize for 10min. After stabilization, baseline data were collected, including the HR, Peak LV systolic pressure (LVESP), LV end-diastolic pressure (LVEDP), and maximal rates of LV pressure rise (dP/dt_{max}) and fall (dP/dt_{min}).² For the pressure volume relationship, the recording from Millar catheter was synchronized with echocardiography measurements as per manufacturer instructions.

Measurement of transketolase activity

Frozen heart tissue was defrosted, chopped finely and a 10% homogenate was prepared with 0.1M Tris-HCl buffer (pH 8.0) and centrifuged at 3,000 x g for 10 min. The lysate was kept on ice until used. For erythrocytes, peripheral blood samples were centrifuged (2,000 x g, 5 min) and the plasma and white blood cells were removed. The packed erythrocytes pellet was washed three times with PBS and lysed with ddH₂O and membrane fragments sedimented (10,000 x g, 10 min, 4°C). The activity of transketolase in myocardial tissue homogenate and erythrocytes lysate was determined by the method of Chamberlain *et al.*^{3, 4} Aliquot (200 µl) of substrate cocktail (14.8 mM R-5-P, 253 µM NADH, 185 U/ml TPI, and 70 µl of 21.5 U/ml GDH in 250 mM Tris/HCl buffer, pH 7.8, all from Sigma Chemical, UK) was added to the wells of a 96-well microplate and 20 µl of a 6-fold dilution of erythrocyte lysate or tissue homogenate was added. The absorbance at 340 nm was monitored at 10 min intervals for 120 min and the rate of decrease in absorbance between 10 to 80 min was used to deduce the rate of oxidation of NADH in the GDH catalyzed reaction, which is rate limited by the transketolase catalyzed conversion of R-5-P and xylulose-5-phosphate to sedoheptulose-7-phosphate and GA3P under these conditions.

Measurement of glucose-6-phosphate dehydrogenase (G6PD) activity

G6PD activity was determined by measuring the rate of production of NADPH as previously described.^{5, 6} In brief, the samples were prepared in a similar manner explained above for transketolase activity. Aliquot (250µl) of substrate cocktail (50 mM glycylglycine, pH 7.4, 2 mM D-glucose-6-phosphate, 100mM 6-phosphogluconic acid, 670 µM βNADP and 10mM MgCl₂)

was added to the wells of a 96-well microplate and 12.5 μ l of a 6-fold dilution of myocardial tissue homogenate or erythrocyte lysate was added. The absorbance at 340 nm was monitored at 1min intervals for 5min. A second 12.5 μ l of a 6-fold dilution of erythrocyte lysate or tissue homogenate was added to a separate substrate cocktail (250 μ l) without D-glucose-6-phosphate and the absorbance was measured for 5 min. G6PD activity was calculated by subtracting the rate of change of absorbance with or without D-glucose-6-phosphate to eliminate the contribution of 6-phosphogluconate dehydrogenase (6PGD) to total NADPH production, as 6PGD also produces NADPH. Protein content in each sample was measured by BioRad assay with commercially available kit (BioRad, UK). Data are represented as units/min/ml for erythrocytes and units/min/mg of protein for myocardial homogenates.

Measurement of glyceraldehyde-3-phosphate dehydrogenase (GAPDH) activity

GAPDH activity was measured using the cytosolic fraction of myocardial tissue homogenate, which is prepared by centrifuging the myocardial tissue lysate at 100,000 x g at 4°C for 30 min. Enzyme activity was measured as described earlier.⁷ Briefly, 1 μ g of cytosolic protein was added to 200 μ l of assay buffer (100mM Tris/HCl pH 8.6, 1.5mM NAD, 3mM dithiothreitol, 5mM sodium arsenate, 1.5mM glyceraldehydes-3-phosphate) at room temperature. NADH formed was determined by monitoring the increase in absorbance at 340 nm at 10 sec interval for 1 min and then every minute for 60 min. Activity was expressed as units/sec/mg of protein.

Measurement of blood flow using fluorescent microspheres

Myocardial perfusion was measured using fluorescent microspheres. A polyethylene (PE10) catheter was inserted through the right carotid artery for the reference blood withdrawal. Microspheres, 0.02 μ m in diameter (Molecular Probes, CA, USA) were injected into the LV cavity over 1 min and flushed with 0.15 ml of 0.9% NaCl. Reference blood was collected *via* the carotid catheter starting 15 sec before to 1 min after the microsphere injection. The animals were sacrificed 2 min later and the heart was removed and separated into LV, RV and septum. The kidneys were also collected and analyzed as internal control organs to demonstrate homogenous distribution of the microspheres throughout the bloodstream. Each sample was weighed, cut into

small pieces and digested in 10 ml of 2 M ethanolic KOH containing 0.5% Tween 80 at 60°C for 48h with constant shaking. After complete digestion of tissues, the microspheres were collected by centrifugation at 2,000 x g for 20 min and sequential washing with 10 ml of deionized water with or without 0.25% Tween 80. Finally, microspheres were dissolved in 3 ml of 2-ethoxyethylacetate and the fluorescence intensity was determined using a fluorophotometer (Fluostar Optima, BMG labtech). Regional blood flow was calculated as the absolute blood flow in ml/min/g of tissue as described earlier.⁸

Assessment of myocardial capillary and arteriole densities

LV sections (3µm) were deparaffinized and incubated with biotinylated Isolectin B4 (Invitrogen, Molecular Probes) followed by streptavidin Alexa Fluor 488 (Invitrogen, Molecular probes) for measurement of capillary density. To measure arteriole density, the sections were incubated with anti-mouse α -smooth muscle cell actin antibody (Sigma chemicals) conjugated with Alexa Fluor 488 (Invitrogen, Molecular probes). Capillaries and arterioles were calculated in at least 20 fields at X400 magnification and the final data expressed as the number of capillaries or arterioles per square millimeter. Arterioles were also categorized according to their luminal size.⁹

Assessment of myocardial fibrosis

Myocardial fibrosis was analyzed by Sirius red staining followed by morphometric analysis using the Image Pro analysis software (MediaCybernetics, USA) and the data expressed as the ratio between intensity of staining and area examined.

TUNEL staining

Apoptosis was quantified on paraffin embedded LV sections (3µm) by the terminal deoxynucleotidyltransferase (TdT)-mediated dUTP nick-end labeling (TUNEL) technique (in situ cell death detection kit Fluorescein, Roche applied science, USA). Following treatment of slides with proteinase K (20 µg/ml, 30min at 37°C), TUNEL assay was performed according to the manufacturer's instruction. The same sections were then stained with DAPI to recognize nuclei. To recognize cardiomyocytes, sections were also stained with mouse monoclonal primary

antibody for the cardiomyocyte marker α -sarcomeric actin (Dako, 1: 50, overnight at 4°C), which was revealed by counterstaining with the secondary antibody conjugated to fluorophore (Alexa 568, Invitrogen, Molecular probes). Twenty fields were randomly evaluated in each section at X400 magnification. The fraction of TUNEL positive nuclei over total cardiomyocyte nuclei was then calculated.¹⁰

In situ detection of reactive oxygen species

Dihydroethidium staining for detection of superoxide

Superoxide production in the myocardium was determined using the fluorescent dye dihydroethidium (DHE, Invitrogen, Molecular probes). LV cryosections (10 μ m) were incubated with 5 μ mol/L DHE, at 37°C for 30 min, in a humidified chamber. Images (X100 magnification) were captured on an Olympus fluorescence microscope fitted with camera (Media cybermatics) and the mean DHE fluorescence intensity of myocyte nuclei was calculated by dividing the combined fluorescence value of the pixels by the total number of pixels in 15 randomly selected field using Image-Pro advanced software.¹¹

8-OHDG staining for detection of hydroxyl radicals

Myocardial production of hydroxyl radicals was determined by immunofluorescent staining of the deparaffinized LV sections (3 μ m) using the primary antibody for 8-hydroxy-2'-deoxyguanosine (8-OHDG, Cosmo Bio, Japan). The nuclear localization of 8-OHDG was detected using the goat anti-mouse secondary antibody conjugated to fluorophore (Alexa 568, Invitrogen, Molecular probes) and counterstaining the cardiomyocytes with α -sarcomeric actin and DAPI to recognize nuclei. Images (X1000 magnification) were captured using an Olympus fluorescence microscope fitted with camera (Media cybernetics, USA) and data expressed as percentage of 8-OHDG positive nuclei.¹²

Immunocytochemical analysis for Akt localization

Effect of HG on localization of Akt was detected using immunocytochemical analysis. For this purpose, HL-1 cells were fixed with 4% paraformaldehyde following exposure to HG for 24h or 72h with or without treatment with BFT. After repeated washing and subsequent blocking with

serum, the cells were incubated with primary antibody against Ser473- phospho-Akt (Cell Signaling, 1:1000) at 4°C overnight. The nuclear or cytoplasmic localization of pAkt was detected using the goat anti-rabbit secondary antibody conjugated to flourophore (Alexa 488, Invitrogen, Molecular probes). Images (X400 magnification) were captured using an Olympus fluorescence microscope fitted with camera (Media cybernetics, USA).

Western blot analyses

Proteins were extracted from LV using ice-cold RIPA buffer. Protein concentration was determined using the Bio-Rad protein assay reagent (Bio-Rad). Detection of proteins by western blot analysis was done following separation of whole tissue / cell extracts (50µg) on SDS-polyacrylamide gels. Proteins were transferred to polyvinylidene difluoride membranes (PVDF, Amersham-Pharmacia) and probed with the following antibodies: anti-mouse Ser 1177-phospho-eNOS (Cell Signaling, 1:1000), eNOS (Cell Signaling, 1:1000), Ser473-phospho-Akt (Cell Signaling, 1:1000), Akt (Cell Signaling, 1:1000), Ser256- phospho-FOXO-1 (Upstate, UK), FOXO-1 (Cell Signaling, 1:1000), Tyr705 phospho-STAT3 (Cell signaling, 1:500), STAT3 (Cell Signaling, 1:1000), Pim-1 (Santacruz biotechnology, 1:250), Ser112-phospho-Bad (Cell Signaling, 1:1000), Bad (Cell Signaling, 1:1000), Bcl-2 (Cell Signaling, 1:1000) and cleaved-caspase-3 (Cell Signaling, 1:1000). Actin (Cell Signaling, 1:1000) was used as loading control. For detection, secondary antibody goat anti-rabbit or anti-mouse conjugated to horseradish peroxidase (both from Amersham Pharmacia, 1:5000) were used, followed by chemiluminescence reaction (ECL, Amersham Pharmacia).

RT-PCR

Total RNA was isolated from LV samples as well as from HL-1 cells (Trizol, Invitrogen, UK) and reverse transcribed (Sensiscript reverse transcriptase, Qiagen). Quantitative PCR (qPCR) was performed in a LightCycler (Roche, Burgess Hill, UK) using Platinum taq polymerase (Qiagen) and the primer pairs listed below. For quantification, mRNA amount of the respective gene was normalized to the amount of 18S rRNA using the 2- $\Delta\Delta$ CT method. Each reaction was performed in triplicate.¹³

<i>18S rRNA</i>	ward: 5' - TAGAGGGACAAGTGGCGTTC -3' verse: 5' - TGTACAAAGGGCAGGGACTT -3'
Pim-1	ward: 5' - TCTCAGGGACAGGCACCATT -3' verse: 5' - GCGGCGAAATCAAACATC -3'

In vitro inhibition of PI3K and Akt

To verify the involvement of PI3K/Akt in BFT-induced pro-survival effects, we used two protocols. In the first protocol, HG-treated HL-1 cardiomyocytes were exposed to the PI3K inhibitor LY-294002 (50 μ M, Sigma Aldrich)¹⁰ for 24h followed by treatment with BFT (150 μ M) or vehicle (1mM HCl). In the second protocol, HG-treated HL-1 cardiomyocytes were infected with an adenovirus carrying a HA-tagged dominant negative mutated form of Akt (*Ad.DN-Akt*, K179M) or control *Ad.Null* (both at 100MOI).¹⁰ After 24h, the medium was replaced with a fresh one supplemented with either BFT or vehicle. After additional 24h, cells were used for measurements of caspase-3/7 activity (6 wells per each condition and repeated 3 times) and western blot (WB) analyses (n=4 samples per group).

References

1. de Simone G, Wallerson DC, Volpe M, Devereux RB. Echocardiographic measurement of left ventricular mass and volume in normotensive and hypertensive rats. Necropsy validation. *Am J Hypertens*. 1990;3:688-696.
2. Spillmann F, Graiani G, Van Linthout S, Meloni M, Campesi I, Lagrasta C, Westermann D, Tschöpe C, Quaini F, Emanuelli C, Madeddu P. Regional and global protective effects of tissue kallikrein gene delivery to the peri-infarct myocardium. *Regen Med*. 2006;1:235-254.
3. Chamberlain BR, Buttery JE, Pannall PR. A stable reagent mixture for the whole blood transketolase assay. *Ann Clin Biochem*. 1996;33 (Pt 4):352-354.
4. Buttery JE, Milner CR, Chamberlain BR. Correction for the suppressive effect of haemoglobin on NADH absorbance in the transketolase assay. *Clin Chim Acta*. 1980;102:221-225.
5. Zhang Z, Apse K, Pang J, Stanton RC. High glucose inhibits glucose-6-phosphate dehydrogenase via cAMP in aortic endothelial cells. *J Biol Chem*. 2000;275:40042-40047.
6. Li X, Xu Z, Li S, Rozanski GJ. Redox regulation of Ito remodeling in diabetic rat heart. *Am J Physiol Heart Circ Physiol*. 2005;288:H1417-1424.
7. Tao Y, Howlett A, Klein C. Nitric oxide regulation of glyceraldehyde-3-phosphate dehydrogenase activity in Dictyostelium discoideum cells and lysates. *Eur J Biochem*. 1994;224:447-454.
8. Smith RS, Jr., Gao L, Chao L, Chao J. Tissue kallikrein and kinin infusion promotes neovascularization in limb ischemia. *Biol Chem*. 2008;389:725-730.
9. Stone OA, Richer C, Emanuelli C, van Weel V, Quax PH, Katare R, Kraenkel N, Campagnolo P, Barcelos LS, Siragusa M, Sala-Newby GB, Baldessari D, Mione M, Vincent MP, Benest AV, Al Haj Zen A, Gonzalez J, Bates DO, Alhenc-Gelas F, Madeddu P. Critical Role of Tissue Kallikrein in Vessel Formation and Maturation. Implications for Therapeutic Revascularization. *Arterioscler Thromb Vasc Biol*. 2009.
10. Caporali A, Sala-Newby GB, Meloni M, Graiani G, Pani E, Cristofaro B, Newby AC,

- Madeddu P, Emanuelli C. Identification of the prosurvival activity of nerve growth factor on cardiac myocytes. *Cell Death Differ*. 2008;15:299-311.
11. Kumashiro N, Tamura Y, Uchida T, Ogihara T, Fujitani Y, Hirose T, Mochizuki H, Kawamori R, Watada H. Impact of oxidative stress and peroxisome proliferator-activated receptor gamma coactivator-1alpha in hepatic insulin resistance. *Diabetes*. 2008;57:2083-2091.
 12. Rota M, LeCapitaine N, Hosoda T, Boni A, De Angelis A, Padin-Iruegas ME, Esposito G, Vitale S, Urbanek K, Casarsa C, Giorgio M, Luscher TF, Pelicci PG, Anversa P, Leri A, Kajstura J. Diabetes promotes cardiac stem cell aging and heart failure, which are prevented by deletion of the p66shc gene. *Circ Res*. 2006;99:42-52.
 13. Caporali A, Pani E, Horrevoets AJ, Kraenkel N, Oikawa A, Sala-Newby GB, Meloni M, Cristofaro B, Graiani G, Leroyer AS, Boulanger CM, Spinetti G, Yoon SO, Madeddu P, Emanuelli C. Neurotrophin p75 receptor (p75NTR) promotes endothelial cell apoptosis and inhibits angiogenesis: implications for diabetes-induced impaired neovascularization in ischemic limb muscles. *Circ Res*. 2008;103:e15-26.

Legends to Supplemental Figures

Supplemental Figure 1

Illustration of experimental protocols in type-1 (A) and type-2 (B) diabetic mice. Animals were randomized in subsequent phases for: (1) treatment with BFT or vehicle (4 weeks after the last STZ injection throughout duration of the study), (2) echocardiography/survival follow up or molecular biology assessment at indicated time points and (3) terminal measurement of intra-ventricular pressure or measurement of cardiac perfusion, or sampling of the heart for histology. *In type-1 DM protocol, 120 mice showing overt glycosuria entered the study, while the remaining 20 were discarded because of unsuccessful induction of DM.

The same protocol was carried out in parallel in (1) age-matched mice (healthy controls of type-1 DM), which were injected with the STZ-vehicle and 4 weeks later were randomly allocated to treatment with BFT or its vehicle (n=40 each) and (2) age-matched lean mice (BKS.Cg-m+/+Lepr^{db}/OlaHsd, db/+) which were randomly allocated to treatment with BFT or its vehicle at 9 weeks of age (n=14 each)

Supplemental Figure 2

Scatter plots show the serum glucose levels in type-1 (A) and type-2 (B) diabetic mice during treatment with BFT or vehicle. **P<0.001 versus respective control healthy mice in type-1 DM or db/+ mice in type-2 DM; #P<0.05 or ##P<0.01 versus pre-treatment (time 0, corresponding to 9 weeks of age) in db/db mice.

Supplemental Figure 3

Bar graphs show the levels of activated caspase-3/7 in cultured adult cardiomyocytes.

A. Cardiomyocytes were cultured in normal glucose (NG) or high glucose (30mM) with different concentrations of benfotiamine (B) or vehicle (V). Values are expressed as relative units (RLU) and are mean \pm standard deviation. *P<0.01 and **P<0.001 versus NG; #P<0.01 versus V.

B. Cardiomyocytes were cultured in normal (5mM D-glucose) or high glucose (15 - 35mM

D-glucose) with 150 μ M benfotiamine or vehicle. Values are expressed as relative units (RLU), and are mean \pm standard deviation. **P<0.001 versus 5mM D-glucose and $^{\$}$ P<0.01 versus corresponding vehicle group.

Each experiment was performed in 6 wells per each condition and repeated 3 times.

Supplemental Figure 4

Echocardiographic assessment of cardiac function in type-1 (A, n=16 in each group) and type-2 diabetic mice (B, n=10 in each group). Upper panels show linear measures of LV cavity captured at end-systole and end-diastole. Lower panels show LV posterior wall thickness at end-diastole and cardiac output. Values are mean \pm standard deviation. BFT did not affect cardiac parameters in healthy mice (data not shown). Results of pair-wise comparison are illustrated: *P<0.01, **P<0.001 and ***P<0.0001 versus vehicle-treated healthy mice in type-1 DM or db/+ mice in type-2 DM; #P<0.01 and ##P<0.001 versus vehicle-treated diabetic mice in type-1 DM or db/db mice in type-2 DM. End systolic LV chamber internal diameter values of healthy and diabetic-BFT mice from 4 and 12 weeks overlapped and are therefore expressed by the same line.

Supplemental Figure 5

(A) Line graphs show changes in the maximum (inotropic) and minimum (lusitropic) rates of developed pressure in response to adrenergic stimulation (epinephrine 1mg/kg/IV) in healthy and type-1 diabetic mice, given BFT or vehicle. (B) Average response to adrenergic stimulation is expressed as area under the curve. Values are mean \pm standard deviation. Results of pair-wise comparison are illustrated: *P<0.01 versus vehicle-treated healthy mice; #P<0.01 versus vehicle-treated diabetic mice. Each group consisted of 6 mice.

Supplemental Figure 6

Line graph shows the effect of BFT on survival of type-1 diabetic mice. Mice were followed until 20 weeks after STZ (n=32 vehicle-treated or BFT-treated diabetic mice) or STZ-vehicle injection (n=40 healthy mice). Diabetic mice showed an increased mortality (P<0.001 versus

healthy mice), which was prevented by BFT ($P < 0.001$ versus vehicle-treated diabetic mice). The survival rate of type-2 diabetic mice was not determined because of the limited group size.

Supplemental Figure 7

Representative microphotographs and bar graphs show the effect of BFT on superoxide levels in myocardium at 20 weeks from STZ or STZ-vehicle injection in type-1 diabetic mice. Each group consisted of 5 mice. Values are mean \pm standard deviation. Results of pair-wise comparison are illustrated: * $P < 0.001$ and ** $P < 0.001$ versus healthy mice; ### $P < 0.001$ versus vehicle-treated diabetic mice. Scale bars are 100 μ m.

Supplemental figure 8

(A-B) Bar graphs show the levels of *Pim-1* gene expression in LV of type-1 (at 8, 12 and 20 weeks from STZ or STZ-vehicle injection, A) or type-2 diabetic mice (at 13 and 17 weeks of age, B). Each group consisted of 4 mice. Values are expressed as n-fold changes toward vehicle-treated healthy mice and are mean \pm standard deviation. * $P < 0.01$ and ** $P < 0.001$ versus healthy mice in type-1 DM or db/+ mice in type-2 DM; # $P < 0.01$ and ### $P < 0.01$ versus vehicle-treated diabetic mice in type-1 DM or db/db mice in type-2 DM. (C) Bar graphs showing the levels of *Pim-1* gene expression in cultured adult cardiomyocytes. Cardiomyocytes were cultured in normal (NG) or high glucose (HG) in the presence of benfotiamine (HGB) or vehicle. Each experiment was repeated three times in triplicate. Values are expressed as n-fold changes toward NG and are mean \pm standard deviation. * $P < 0.01$ versus NG; # $P < 0.01$ versus HG.

Supplemental Figure 9

(A-I) Bar graphs show the levels of activated caspase-3/7 (A), *Pim-1* (B), pBad (C), Bcl-2 (D), pSTAT3 (E), pAkt (F), Akt kinase activity (G), peNOS (H) and pFOXO-1 (I) in cultured adult cardiomyocytes. Cardiomyocytes were cultured in normal (NG) or high glucose (HG) in the presence of benfotiamine (NGB and HGB) or vehicle. Each experiment was repeated three times in triplicate. Values are expressed as n-fold changes toward NG for all parameters, except caspase 3/7 which is expressed as relative units (RLU), and are mean \pm standard deviation. Siegel-Tukey test detected statistical differences as illustrated: * $P < 0.01$ and ** $P < 0.001$ versus

NG; [#]P<0.01 and ^{##}P<0.001 versus HG. (J) Representative microphotographs showing the pAkt intracellular localization in cardiomyocytes cultured in normal (NG) or high glucose (HG) for 24 or 72 h in presence of benfotiamine (HGB) or vehicle. Scale bars are 50 μ m.

Supplemental Figure 10

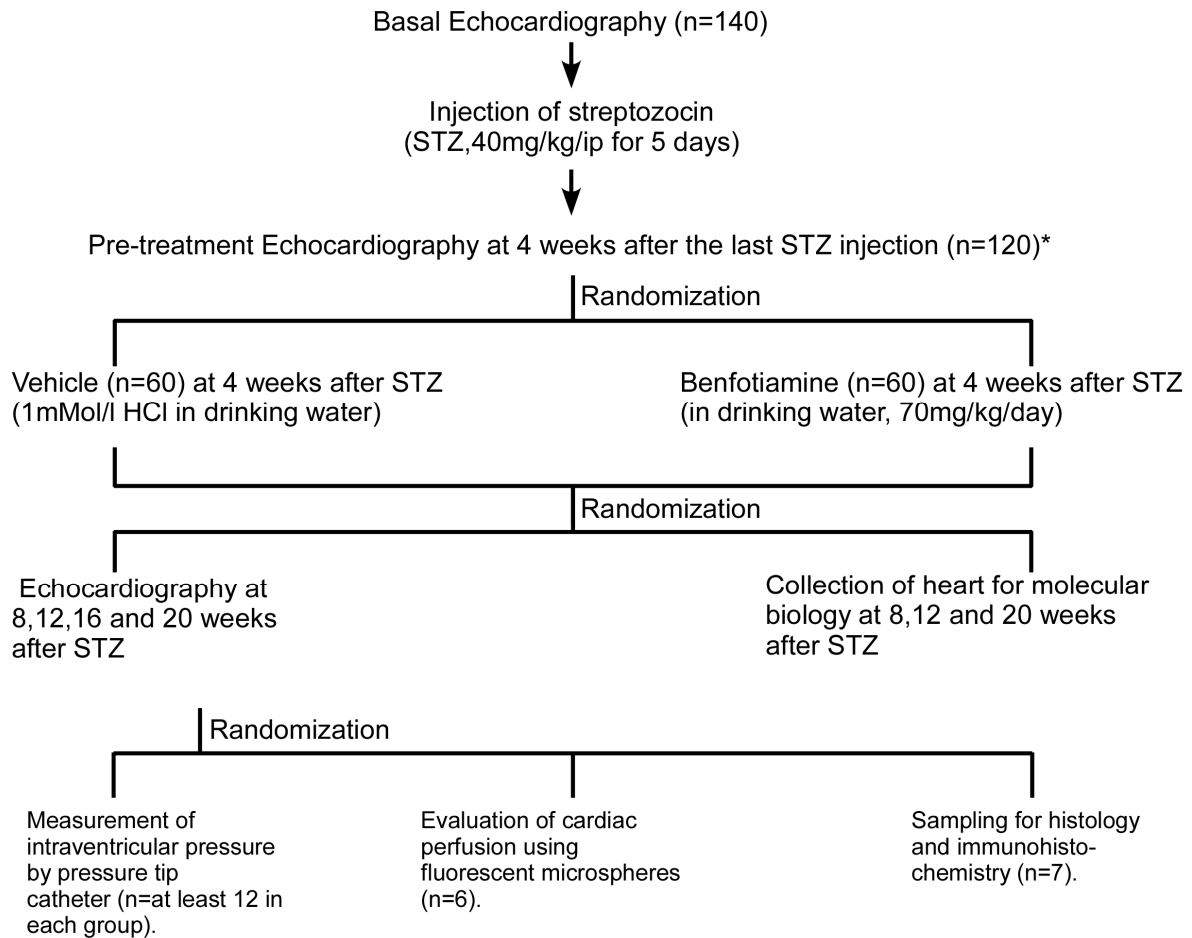
(A-F) Bar graphs show the levels of pSTAT3 (A), pAkt (B), Pim-1 (C), pBad (D) Bcl-2 (E) and activated caspase-3/7 (F). Cardiomyocytes cultured in high glucose (HG) or normal glucose (NG) were infected with *Ad.DN-Akt* or *Ad.Null* followed by another 24h culture in the presence of benfotiamine (HGB) or vehicle. Each experiment was performed in triplicate and repeated three times. For caspase-3/7 activity, assay was performed in 6 wells per each condition and repeated three times. Values are expressed as n-fold changes toward *Ad.Null* NG for all parameters, except for caspase 3/7, which is expressed as relative units (RLU), and are mean \pm standard deviation. *P<0.01 and **P<0.001 versus NG within *Ad.DN-Akt* or *Ad.Null* groups; [#]P<0.01 and ^{##}P<0.001 versus HG within *Ad.DN-Akt* or *Ad.Null* groups. ^{\$}P<0.01 versus the corresponding treatment of the *Ad.Null* group. (G) Bar graphs show the levels of activated caspase-3/7 in cultured adult cardiomyocytes exposed to high glucose in the presence of LY 294002 (50 μ M) or vehicle. Each experiment was performed in 6 wells per each condition and repeated three times. Values expressed as relative units (RLU), and are mean \pm standard deviation. *P<0.01 and **P<0.001 versus NG within vehicle or LY 294002 groups; [#]P<0.01 versus HG within vehicle group. ^{\$}P<0.01 versus corresponding treatment of the vehicle group. (H-M) Bar graphs show the levels of pSTAT3 (H), pAkt (I), Pim-1 (J), pBad (K) Bcl-2 (L) and activated caspase-3/7 (M) in cultured adult cardiomyocytes. Cardiomyocytes cultured in HG or NG were preincubated with STAT3 inhibitor peptide (1mM) or vehicle for 30 min, followed by another 24 h culture in the presence of benfotiamine (HGB) or vehicle. Values are expressed as n-fold changes toward NG (vehicle) for all parameters, except for caspase 3/7, which is expressed as relative units (RLU), and are mean \pm standard deviation. *P<0.01 and **P<0.001 versus NG within STAT3 inhibitor peptide or vehicle groups; [#]P<0.01 and ^{##}P<0.001 versus HG within STAT3 inhibitor peptide or vehicle groups. ^{\$}P<0.01 versus corresponding treatment of vehicle group.

Supplemental Figure 11

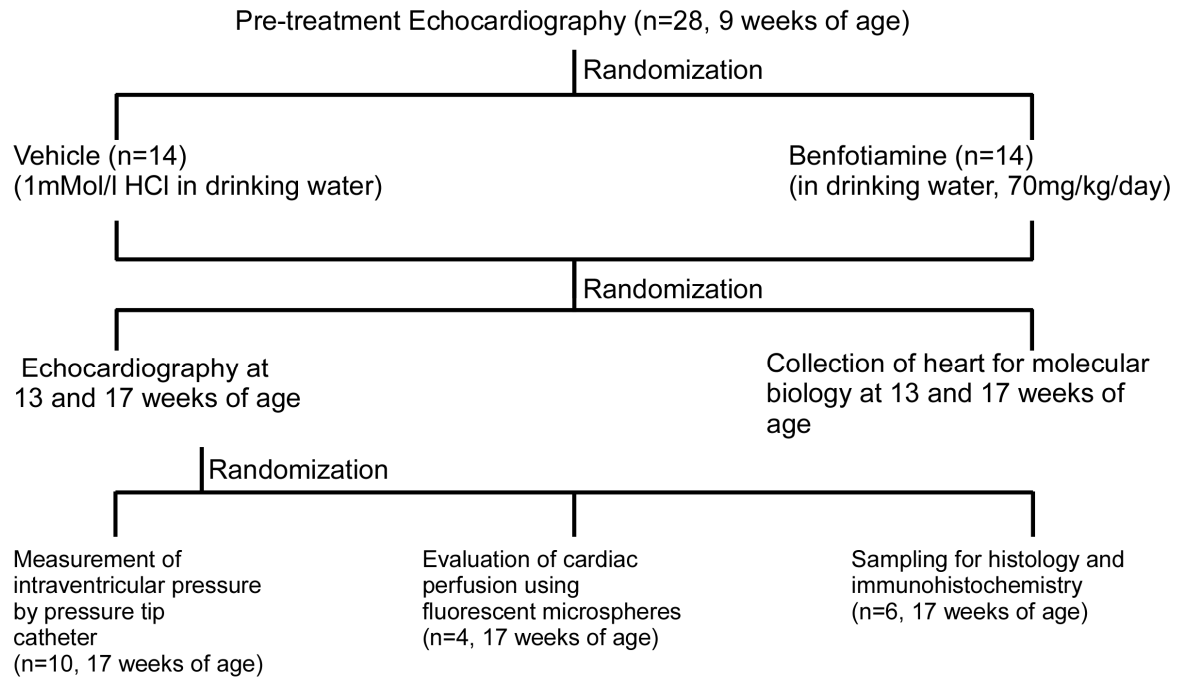
Schematic illustration showing mechanisms implicated in BFT induced cardio-protection in the setting of diabetes.

Diabetes or hyperglycemia inhibits the phosphorylation of STAT3, which is known to activate cell survival Pim-1 by binding to its promoter. Furthermore, diabetes or hyperglycemia induces O-GlcNAC modification of Akt, resulting in inhibition of Akt activity. BFT acts on both arms of this pathway which converges into Pim-1. We found that BFT preserves STAT3 phosphorylation in cardiomyocytes, with this effect, together with Pim-1 upregulation, being abolished by STAT3 inhibitor peptide. In addition, BFT prevents O-GlcNAC modification of Akt, thereby restoring Akt activity and Pim-1 expression. The effect of BFT on Pim-1 expression is abolished by treating cardiomyocytes with dominant negative form of Akt or PI3-kinase inhibitor LY294002. On the other hand, diabetes or hyperglycemia induced the activation of protein phosphatase 2A (PP2A), which is known to dephosphorylate and destabilize Pim-1. However, the upregulation of PP2A was not affected by BFT, suggesting that BFT mainly acts through positive regulators of Pim-1.

Supplemental Figure 1A - Experimental protocol with type-1 DM mice

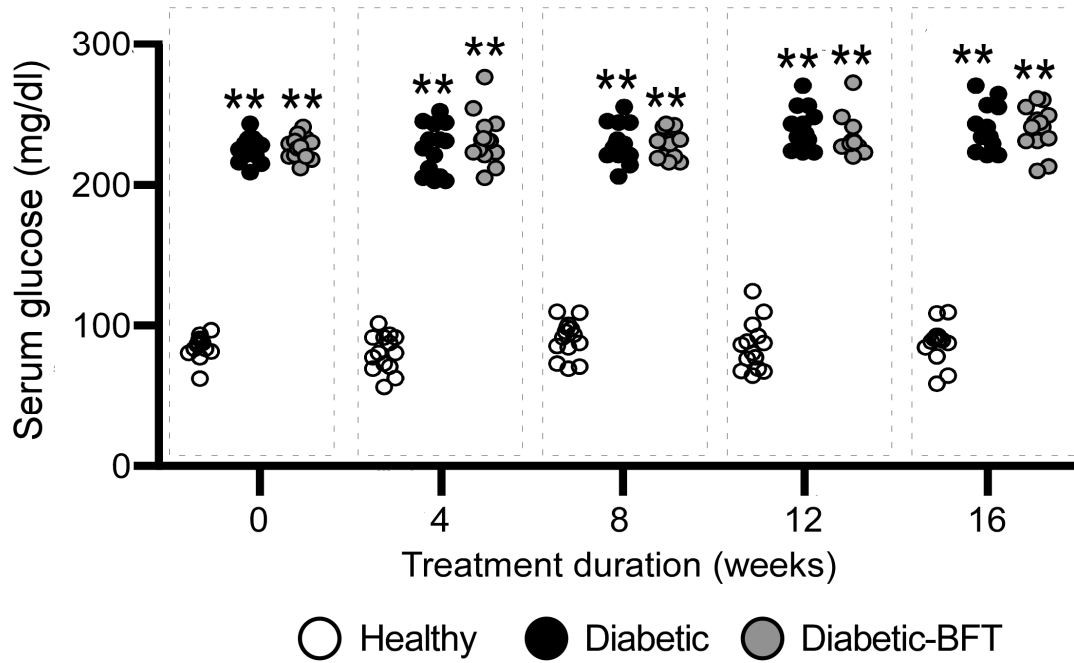


Supplemental Figure 1B - Experimental protocol with type-2 DM mice

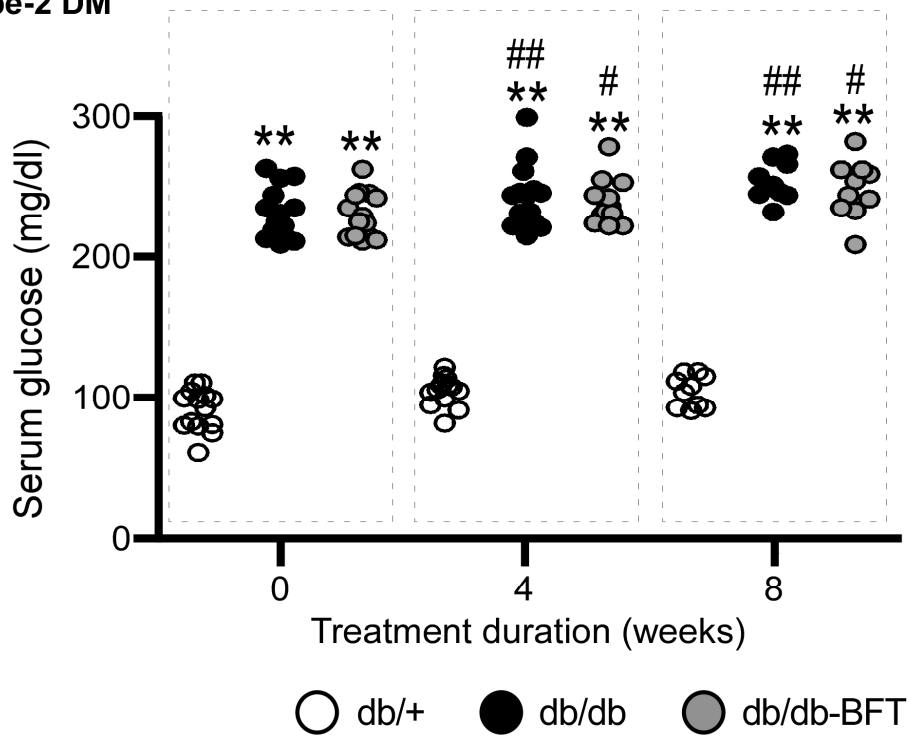


Supplemental Figure 2 - Serum glucose levels

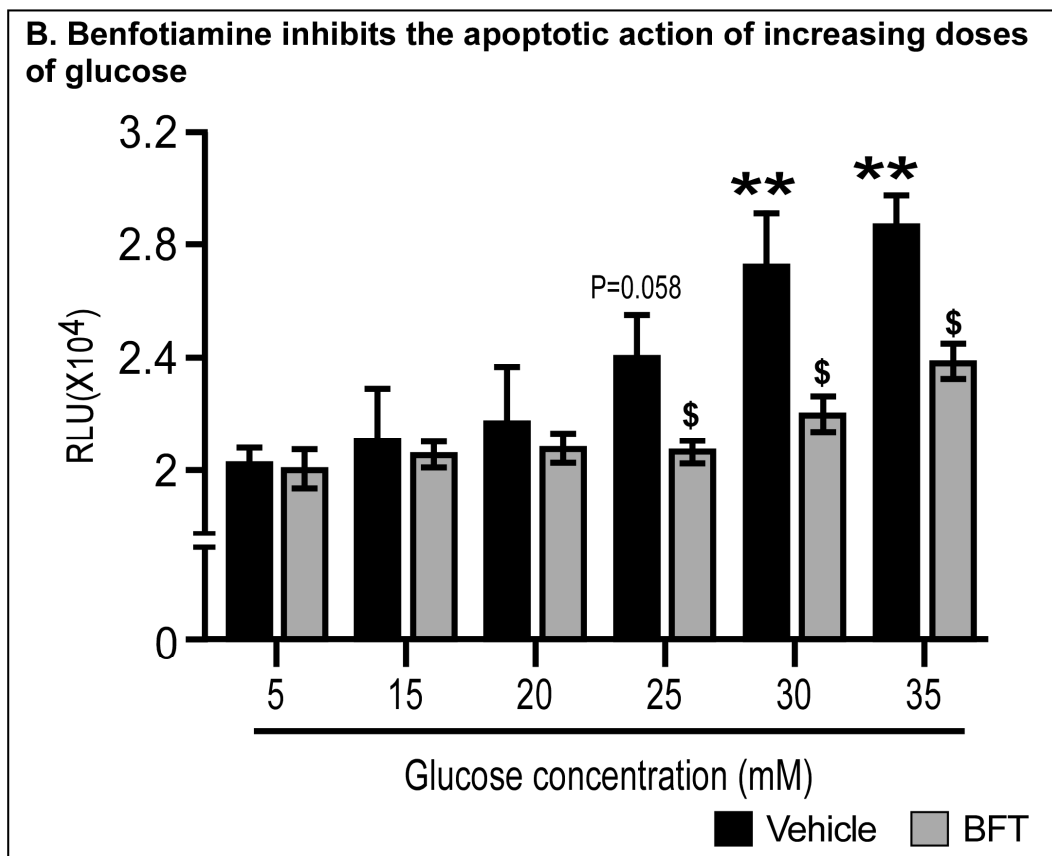
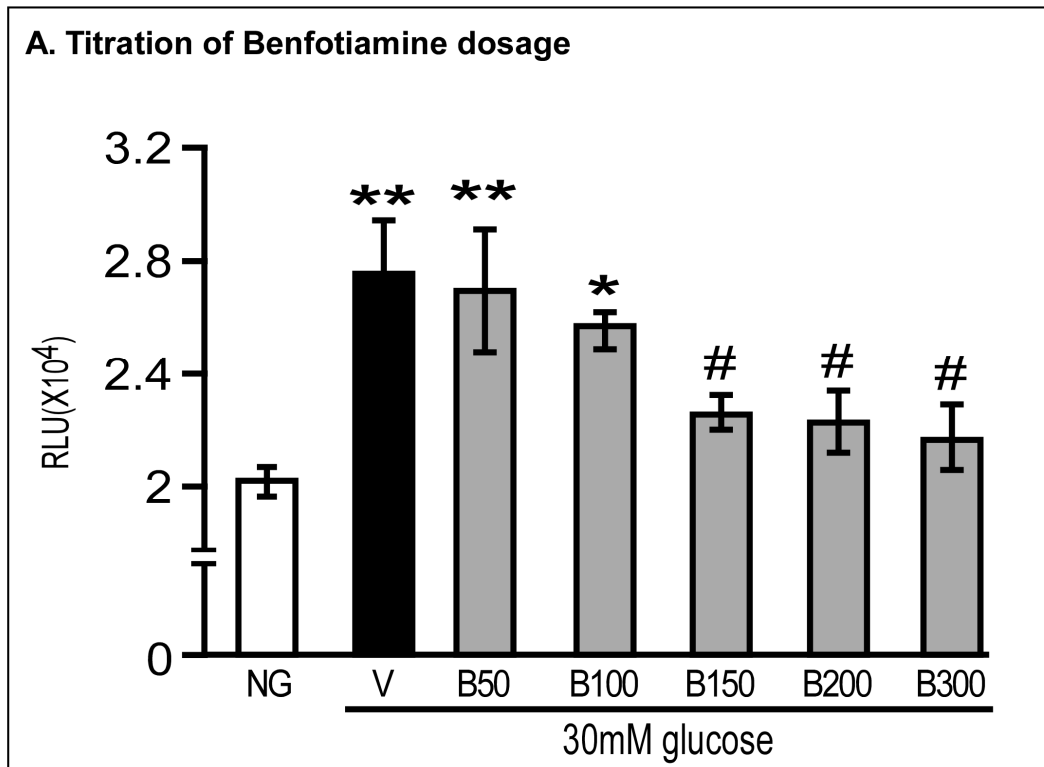
A. Type-1 DM



B. Type-2 DM

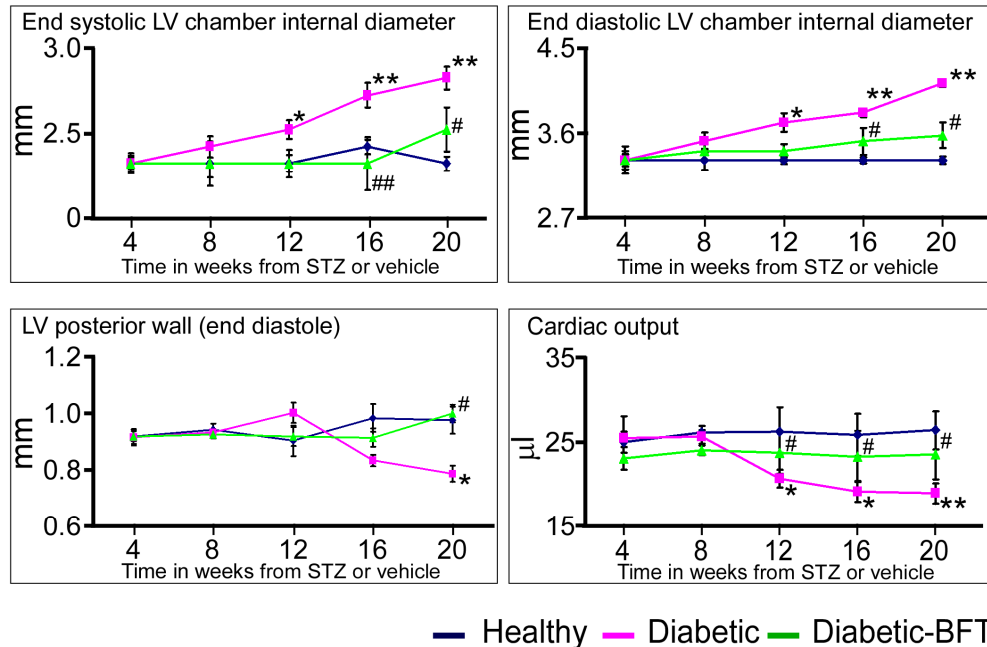


Supplemental Figure 3 - Caspase-glo 3/7 Assay

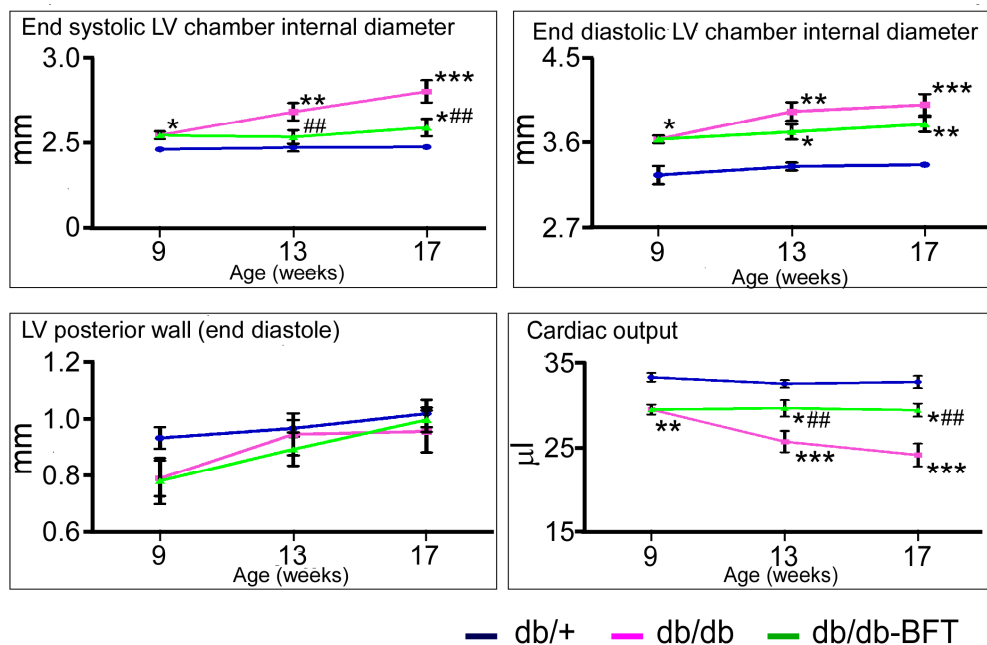


Supplemental Figure 4 - Cardiac function

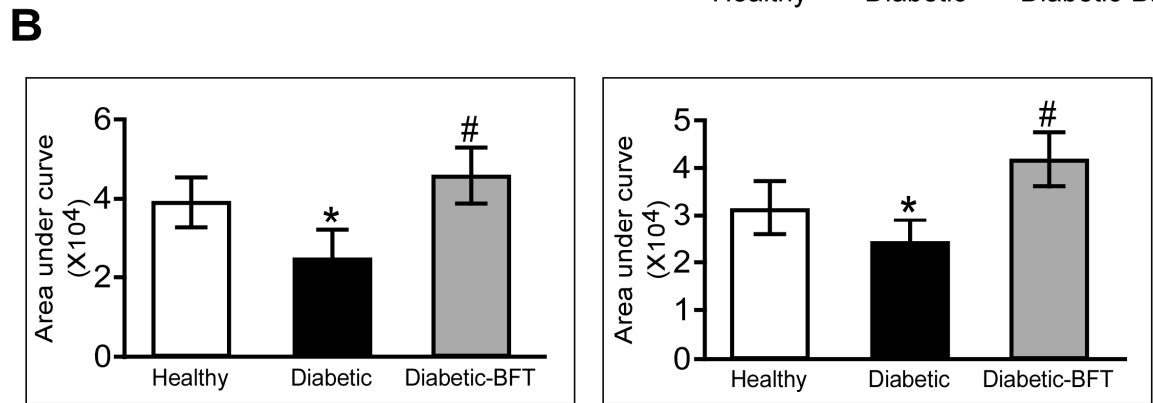
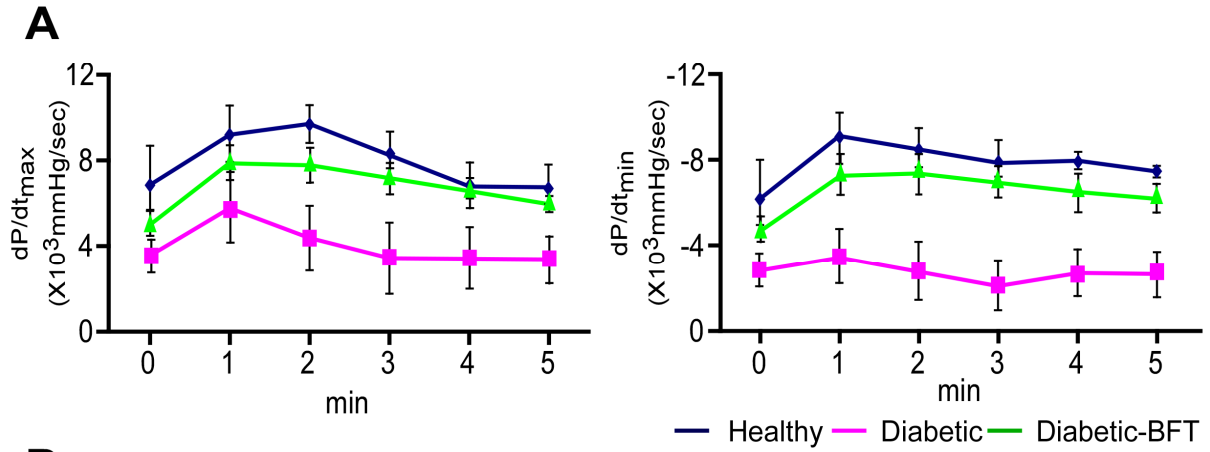
A. Type-1 DM



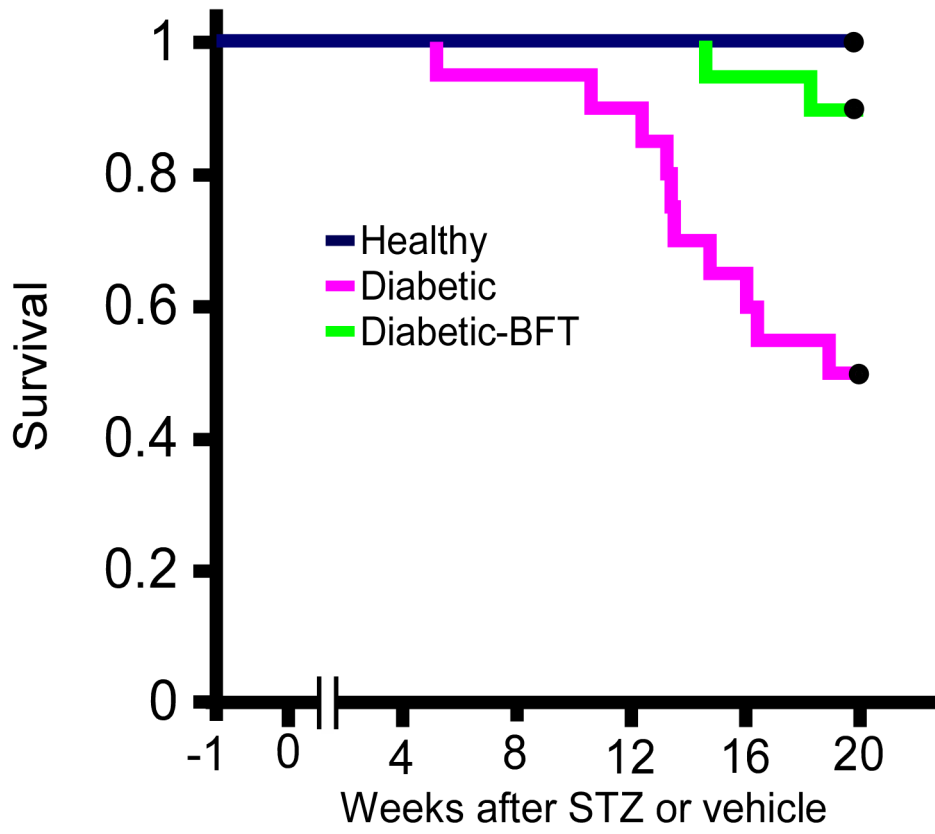
B. Type-2 DM



Supplemental Figure 5

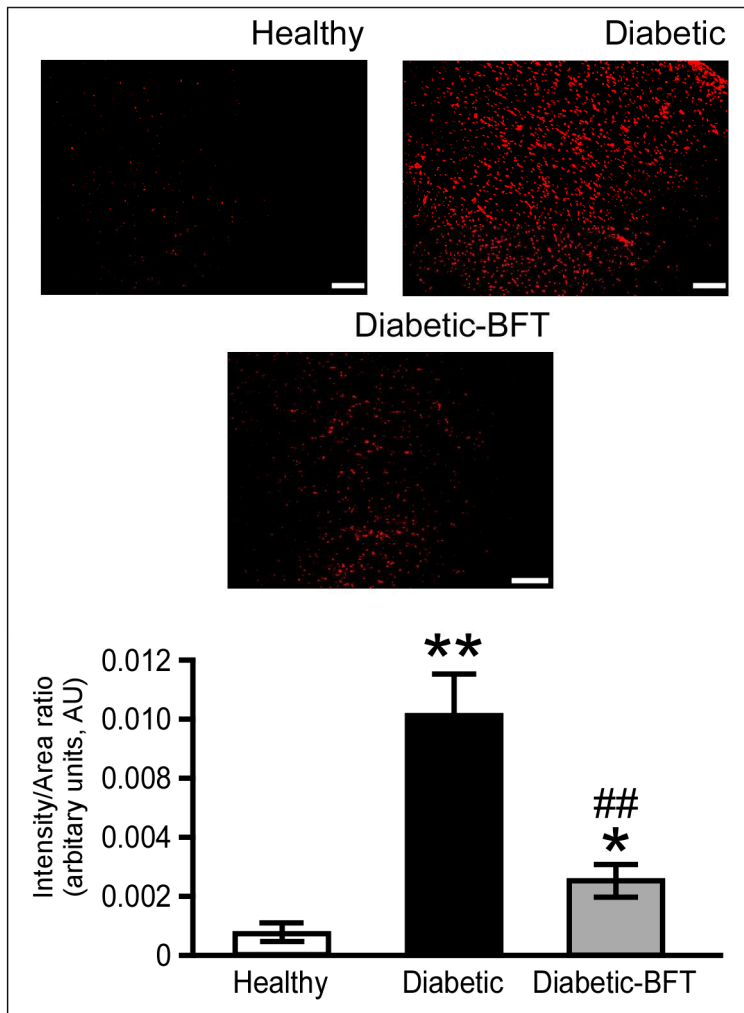


Supplemental Figure 6 - Survival curve

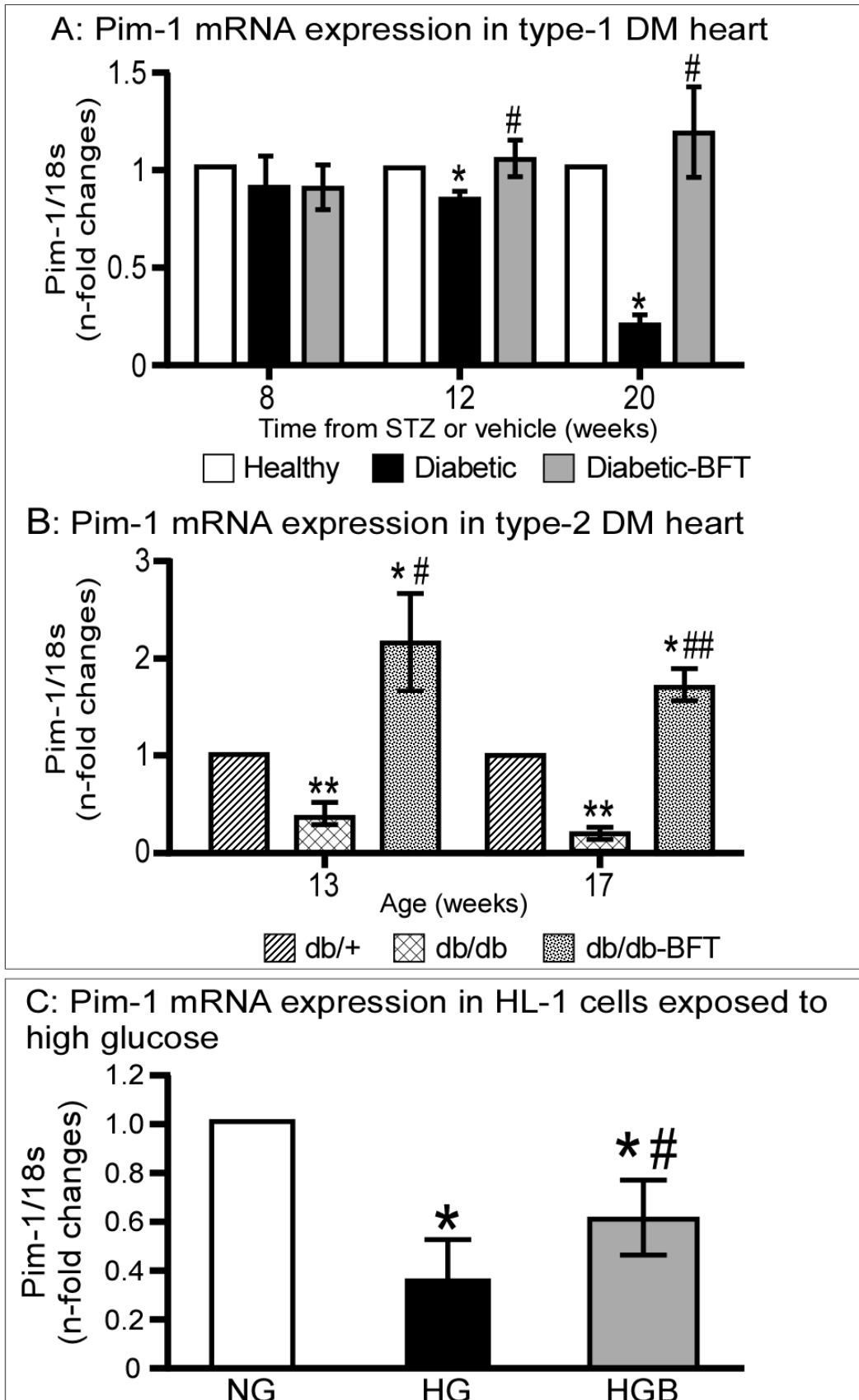


Supplemental Figure 7

DHE staining for superoxides in type-1 DM heart

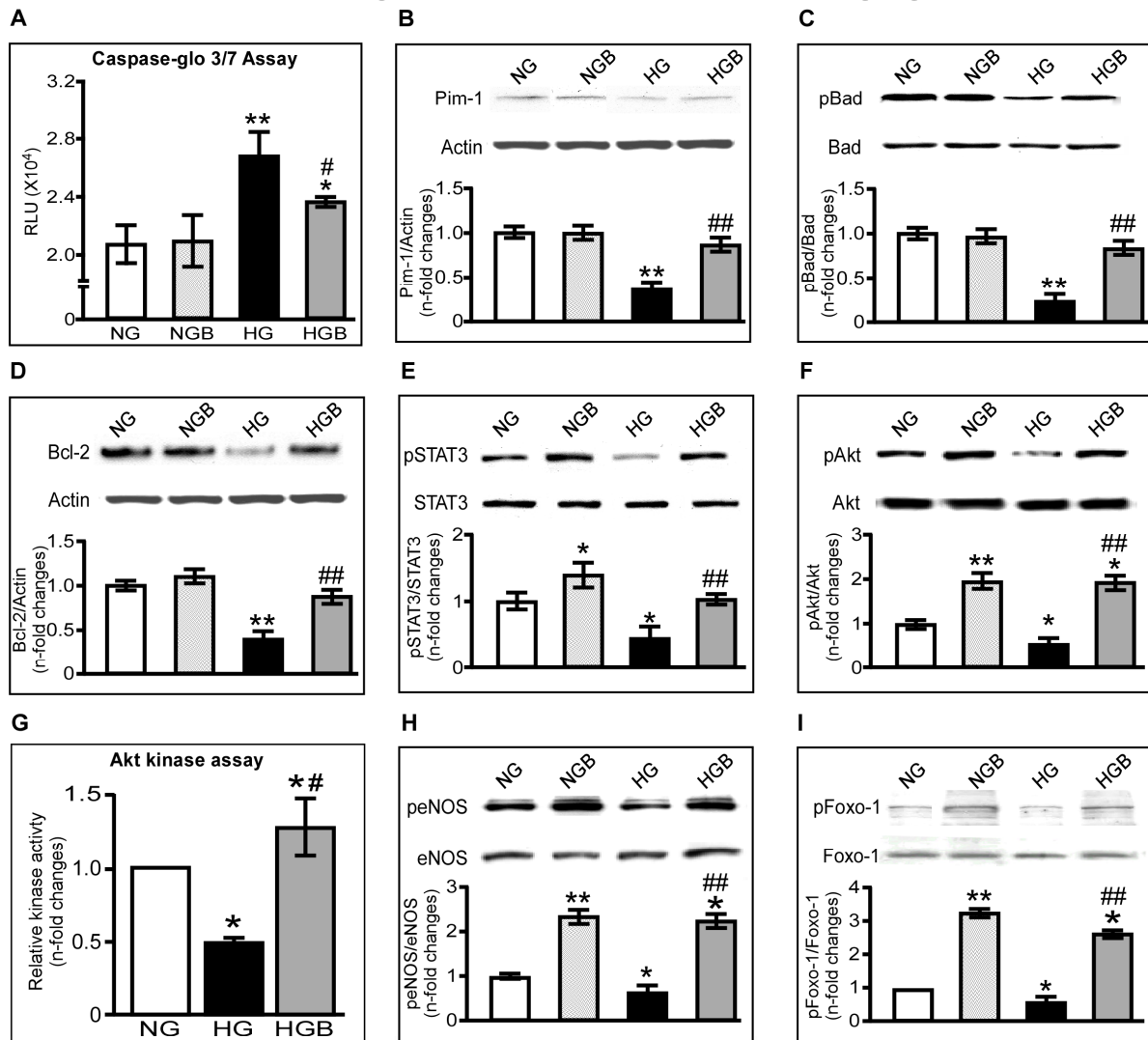


Supplemental Figure 8

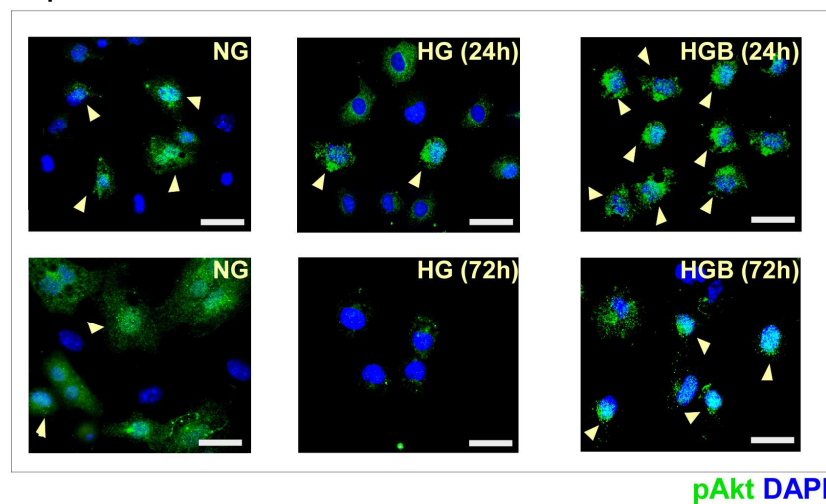


Supplemental Figure 9

Molecular changes in HL-1 cells exposed to high glucose

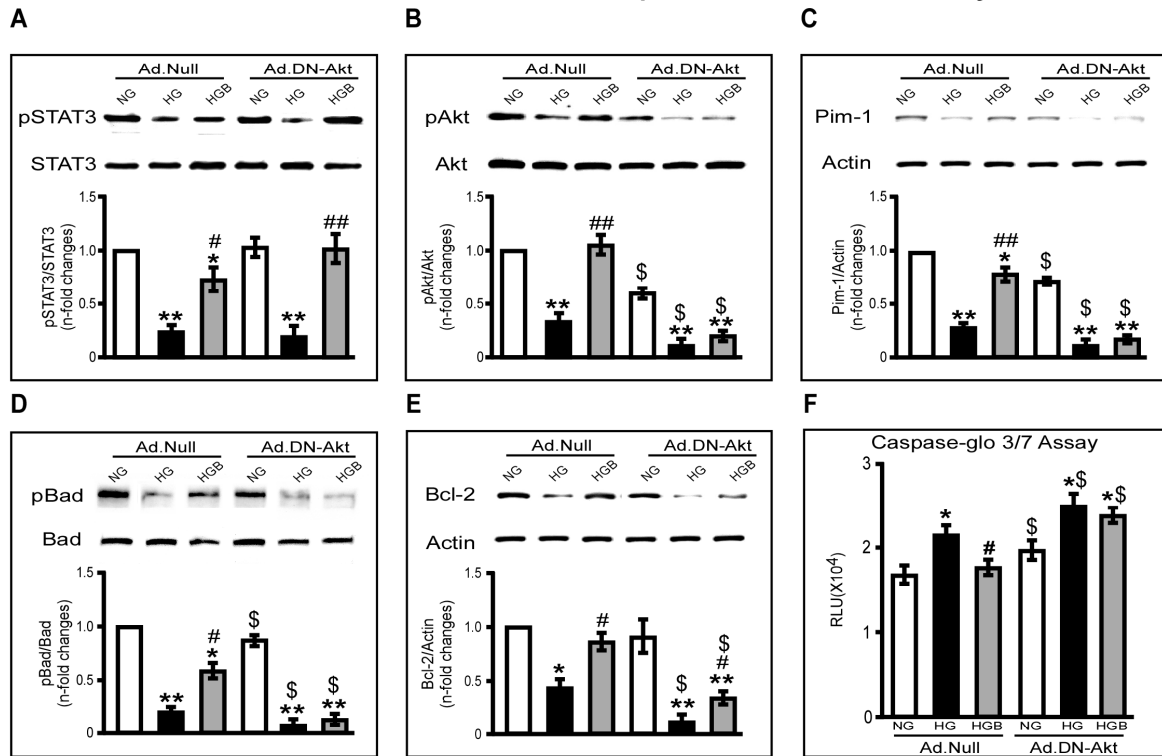


J - pAkt localization

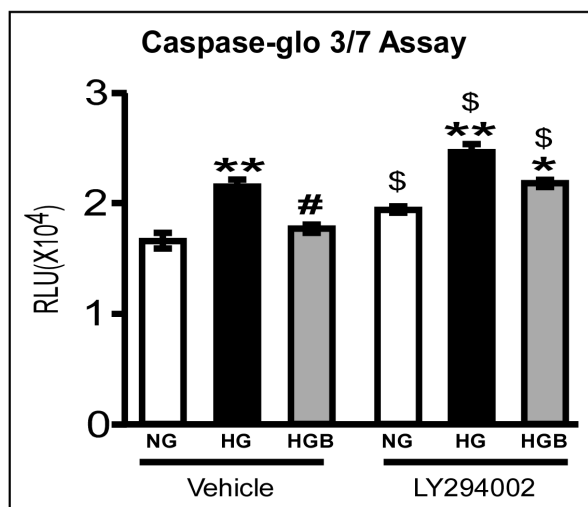


Supplemental Figure 10 (i)

Inhibition of benfotiamine-induced expressional effects by Ad.DN-Akt

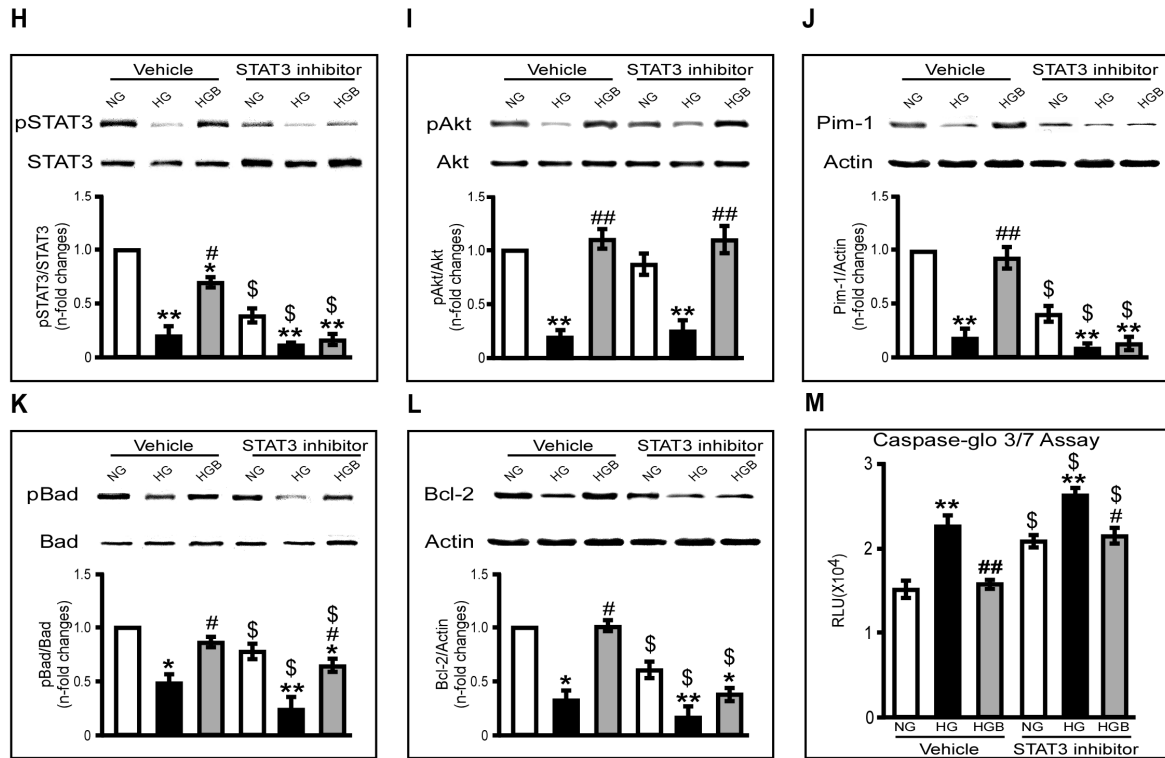


G. Inhibition of benfotiamine-induced pro-survival effects by LY294002



Supplemental Figure 10 (ii)

Inhibition of benfotiamine-induced expressional effects by STAT3 Inhibitor peptide



Supplemental Figure 11

